

# Stability of small-scale UAV helicopters and quadrotors with added payload mass under PID control

Paul E.I. Pounds · Daniel R. Bersak · Aaron M. Dollar

Received: 16 July 2011 / Accepted: 28 January 2012 / Published online: 24 February 2012  
© Springer Science+Business Media, LLC 2012

**Abstract** The application of rotorcraft to autonomous load carrying and transport is a new frontier for Unmanned Aerial Vehicles (UAVs). This task requires that hovering vehicles remain stable and balanced in flight as payload mass is added to the vehicle. If payload is not loaded centered or the vehicle properly trimmed for offset loads, the robot will experience bias forces that must be rejected. In this paper, we explore the effect of dynamic load disturbances introduced by instantaneously increased payload mass and how those affect helicopters and quadrotors under Proportional-Integral-Derivative flight control. We determine stability bounds within which the changing mass-inertia parameters of the system due to the acquired object will not destabilize these aircraft with this standard flight controller. Additionally, we demonstrate experimentally the stability behavior of a helicopter undergoing a range of instantaneous step payload changes.

**Keywords** Unmanned Aerial Vehicle · Quadrotor · Helicopter · Flight stability · Aircraft dynamics

## 1 Introduction

Unmanned Aerial Vehicles (UAVs) have rapidly evolved into capable mobility platforms able to maneuver, navigate and survey with a high degree of autonomy. A natural progression is to advance beyond simple locomotion and observation to physical interaction with objects and the fixed environment. Of specific interest is grasping and retrieving objects while hovering, combining terrestrial robot manipulation capabilities with the range, speed and vertical workspace of flying vehicles. This could make possible novel applications for UAVs, such as search and retrieval in rough or inaccessible terrain, or networked aerial logistical supply chains over large areas.

Along these lines, there is growing interest in the research community towards the development of aerial robotic systems capable of acquiring external payloads or otherwise physically interacting with objects in the environment (Bernard and Kondak 2009; Mammarella et al. 2008; Scott et al. 2007; Bisgaard et al. 2009; Raz et al. 1988; Michael et al. 2009; Amidi et al. 1998; Kuntz and Oh 2008; Borenstein 1992). In our own lab, we have developed the Yale Aerial Manipulator and have demonstrated generalized object retrieval and transport of unstructured objects through the use of a highly adaptive compliant grasper mounted ventrally on the helicopter airframe (Pounds et al. 2011) (see Figs. 1 and 2). This enables the aircraft to acquire a variety of target objects, even in the presence of large positioning errors due to aerodynamic disturbances.

While there are a number of substantial challenges and open research questions related to this application, this pa-

---

A preliminary version of this work was presented at International Conference on Robotics and Automation 2011 (Pounds et al. 2011).

P.E.I. Pounds · D.R. Bersak · A.M. Dollar  
Department of Mechanical Engineering and Materials Science,  
School of Engineering and Applied Science, Yale University,  
New Haven, CT, USA

D.R. Bersak  
e-mail: [daniel.bersak@yale.edu](mailto:daniel.bersak@yale.edu)

A.M. Dollar  
e-mail: [aaron.dollar@yale.edu](mailto:aaron.dollar@yale.edu)

*Present address:*  
P.E.I. Pounds (✉)  
School of Information Technology and Electrical Engineering,  
Faculty of Engineering, Architecture and Information  
Technology, University of Queensland, Brisbane, QLD, Australia  
e-mail: [paul.pounds@uq.edu.au](mailto:paul.pounds@uq.edu.au)



**Fig. 1** Yale Aerial Manipulator carrying a 1.5 kg toolbox in hover



**Fig. 2** Yale Aerial Manipulator with gripper and fixed gear

per focuses on aircraft stability in the presence of large acquired payload objects that cannot be precisely positioned at the center of mass of the vehicle. Unlike full-scale helicopters, a robot vehicle cannot rely on a human to account for instantaneously applied load imbalances and altered trim offsets. The limited intelligence of the aircraft must be sufficient to maintain the stability and desired flight trajectory. Furthermore, most robot vehicles used in research are very small and may be more sensitive to the effects of loads than their larger brethren.

Of particular interest are off-the-shelf Proportional-Integral-Derivative (PID) flight stabilizers that are increasingly available for small-scale helicopter UAVs. It is desirable to employ this class of control system without resort to more complex and expensive custom solutions. Thus it is important to ascertain the suitability and limitations of PID regulators, and show that they will be robust to the dynamic changes and disturbances introduced by adding unbalanced payload to a small helicopter in flight.

We begin the paper by presenting the dynamic model of the longitudinal and pitch dynamics of a helicopter with a PID attitude controller, along with the analytical bounds for object mass and placement for closed-loop stability and cyclic control saturation. In Sect. 3, we provide the numerical results of these bounds for two real helicopters and examine the sensitivity of safe loading distributions for vari-

ations in control parameters and scaling of the robot aircraft. In Sect. 4, we experimentally demonstrate that a PID-stabilized helicopter is robust to a wide range of payload mass and position step disturbances. Finally, in Sect. 5, we analyze the loading bounds of PID-stabilized quadrotor platforms and compare to those of traditional helicopters.

## 2 Helicopter stability with added payload

Adding payload mass to a helicopter changes the dynamic response of the system. The aircraft's flight control system must continue to maintain stability with altered attitude dynamics and must also reject any bias torque induced by a shifted center of mass. If the controller does not maintain stability with changed mass parameters, or cannot reject the step disturbances due to added torque bias from unbalanced loading, the system will be destabilized whenever an object is grasped. This is especially important where a linear commercial off-the-shelf system is used, which may not be adaptable to a changing plant mid-flight. Adding mass to the vehicle slows the natural frequency of the attitude dynamics—this has the advantage of filtering out high-frequency disturbances, but makes it harder to affect fast course corrections.

While several autonomous helicopters have flown with tethered loads (Bernard and Kondak 2009; Bisgaard et al. 2009; Michael et al. 2009), the slung configuration is specifically designed to decouple the motion of the load from the helicopter, and separate the timescales of the attitude and tether-pendulum dynamics (Raz et al. 1988). In the case of grasped and rigidly affixed loads, the payload is directly coupled to vehicle pitch and lateral motions—the closed-loop system must be shown to remain stable in the expected range of system mass and inertia.

### 2.1 Helicopter dynamic model

Much work has been done to control autonomous rotorcraft flight attitude, and the dynamics of helicopters in hover are well understood (Amidi et al. 1998; Pounds et al. 2010; Mettler 2003). Due to the largely decoupled lateral and longitudinal dynamics of helicopters around hover, a planar linear model is useful for analyzing the stability of both the free-air and ground-coupled systems. In this paper, longitudinal dynamics are considered, but the analysis is equally applicable to lateral flight near hover.

The rigid-body dynamics of the linearized planar helicopter in hover are<sup>1</sup> (Fig. 3):

$$m\ddot{x} = -mg\beta - mg\theta - mgu \quad (1)$$

$$I\ddot{\theta} = mgh\beta + mghu + w \quad (2)$$

<sup>1</sup>Rotor thrust is taken as constant, exactly canceling helicopter weight.

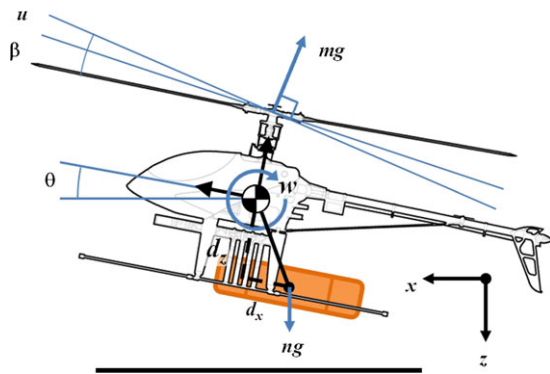


Fig. 3 Planar aircraft dynamics free body diagram

where  $m$  is the mass of the helicopter,  $I$  is the rotational inertia in pitch,  $g$  is acceleration due to gravity,  $x$ ,  $z$  and  $\theta$  are the longitudinal, vertical and angular position of the CoG with respect to the inertial frame,  $h$  is the rotor height above the CoG,  $\beta$  is the first harmonic longitudinal rotor flapping angle,  $u$  is the cyclic pitch control input, and  $w$  is the pitch moment applied by the payload.

All helicopters exhibit rotor flapping (Prouty 2002); we consider a teetering rotor free to pivot at the center like a see-saw. In horizontal motion, the on-coming wind causes an imbalance in lift between the blades on either side of the rotor disc. This causes the rotor plane to pitch upward, changing the angle of attack of each blade until a new equilibrium is reached.

The angled rotor directs some of its thrust aft, slowing the helicopter and producing a pitching moment. Flapping dynamics are a crucial part of helicopter stability analysis, even at low speeds (Pounds et al. 2010). The rotor pitch response time is extremely fast, and so it can be represented analytically, without need for additional states.

At low speeds, the flapping angle produced by a ‘see-saw’ teetering rotor head is an approximately linear combination of the longitudinal translation and pitch velocities:

$$\beta = q_1 \dot{x} - q_2 \dot{\theta} \tag{3}$$

where  $q_1$  and  $q_2$  are constant parameters of the rotor (Pounds et al. 2010).

In the case of rotor heads with Bell-Hiller stabilizer bars, the flapping angle is augmented by that of the sub-rotor, multiplied by the mechanical advantage of the stabilizer linkage transmission  $K$  (Mettler 2003):

$$\beta' = \beta + K(q_{1s} \dot{x} - q_{2s} \dot{\theta}) \tag{4}$$

where  $q_{1s}$  and  $q_{2s}$  are the stabilizer flapping parameters. Together, the stabilized rotor dynamics are homologous to that of a conventional rotor with slower time constants:

$$\beta' = (q_1 + Kq_{1s}) \dot{x} - (q_2 + Kq_{2s}) \dot{\theta} \tag{5}$$

Thus, we need not distinguish between the two in this analysis.

Helicopter pitch and longitudinal motion are strongly interdependent, but vertical motion is effectively decoupled from these around hover. Solving the longitudinal translation-pitch equations together produces a single-input-single-output transfer function between the cyclic control input and the pitch angle in free flight:

$$H = \frac{m^2 g h s}{IGs^2 + mghq_2Gs - m^2g^2hq_1(q_2s - 1)} \tag{6}$$

where  $G = (ms + q_1mg)$ , the dynamics associated with translation due to pitch.

### 2.2 Flight stability with payload mass

Level flight of helicopters is regulated by an onboard flight controller, maintaining  $\theta = 0$ . A common architecture used in UAV rotorcraft is Proportional-Integral-Derivative control. The transfer function for a PID controller has the form:

$$C = k \left( 1 + k_i \frac{1}{s} + k_d s \right) \tag{7}$$

where  $k$  is the control gain, and  $k_i$  and  $k_d$  are the integral and differential control parameters.

The stability of the closed-loop system can be assessed by examining the transfer function characteristic polynomial. The polynomial is the sum of the products of the numerators (subscript  $n$ ) and denominators (subscript  $d$ ) of  $C$  and  $H$ :

$$C_n H_n + C_d H_d \tag{8}$$

Substituting (6) and (7), this becomes:

$$s^3 + \left( \frac{mgh}{I} (q_2 + k k_d) + q_1 g \right) s^2 + k \frac{mgh}{I} s + \frac{mgh}{I} (k k_i + q_1 g) \tag{9}$$

As the unladen helicopter is stable in free air, this polynomial is known to be stable.

Adding payload to the aircraft changes three key parameters:  $m$ , the mass of the helicopter,  $I$ , the rotational inertia of the helicopter, and  $h$ , the height of the rotor plane above the CoG. Changes to these values depend on three attributes of the acquired load:  $n$ , the mass of the payload, and  $d_x$  and  $d_z$ , the longitudinal and vertical offsets of the payload mass from the vehicle CoG. The adjusted parameters are calculated by:

$$m' = m + n \tag{10}$$

$$I' = I + I_n + n(d_x^2 + d_z^2) \tag{11}$$

$$h' = h + \frac{n}{n + m} d_z \tag{12}$$

where  $I_n$  is the rotational inertia of the added payload.<sup>2</sup>

<sup>2</sup>Note that all rotations are considered to occur around the unloaded CoG of the helicopter; offset mass effects are accounted for in the load bias torque.

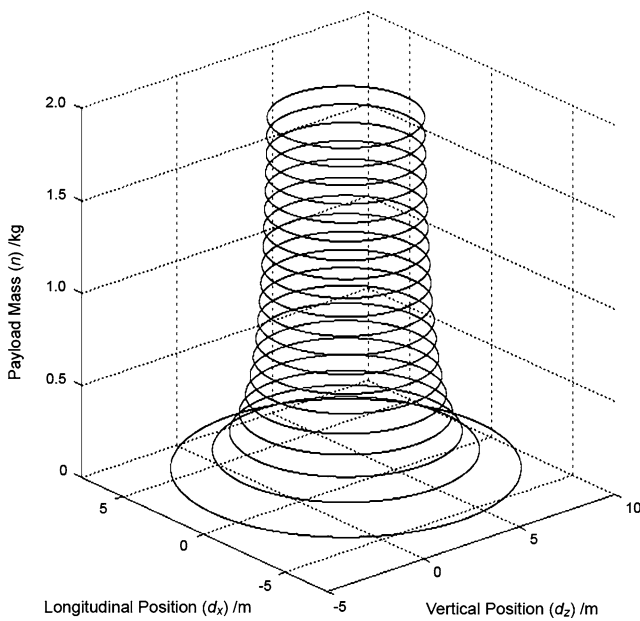


**Fig. 4** Stability region for offset loads isometric with mass isoclines

The continued stability of the characteristic polynomial can be assessed using the Routh-Hurwitz criterion (Pounds and Dollar 2010). The criterion states that for a dynamical system to be stable, its characteristic polynomial must have all positive coefficients, and that leading entries in the Routh-Hurwitz array derived from those coefficients must be positive. In the case of a third order polynomial:

$$s^3 + a_1s^2 + a_2s + a_3 \tag{13}$$

The lead elements of the array are given by:

$$b_1 = (a_1a_2 - a_3)/a_1 \tag{14}$$

$$c_1 = a_3 \tag{15}$$

Mass added to the helicopter is always positive. While in principle  $d_z$  may be arbitrarily positive or negative, the structure of most helicopters precludes adding mass sufficiently far above their centers of gravity such that  $h' < 0$ . Thus, the characteristic polynomial coefficients are always positive.

Therefore, as  $c_1 = a_3$ , only array element  $b_1$  can change signs. From (14) the stability condition becomes:

$$a_1a_2 - a_3 > 0 \tag{16}$$

Substituting the characteristic polynomial coefficients and (10)–(12) and rearranging, this can be expressed as:

$$\frac{m'gh'}{I'} > \frac{q_1g - q_1gk + kk_i}{(q_2 + kk_d)k} \tag{17}$$

Note that the right-hand side of the inequality consists only of constant terms of the aerodynamics and controller; we denote this constant  $P$ . All mass and inertial parameters modified by changing payload appear on the left-hand side of

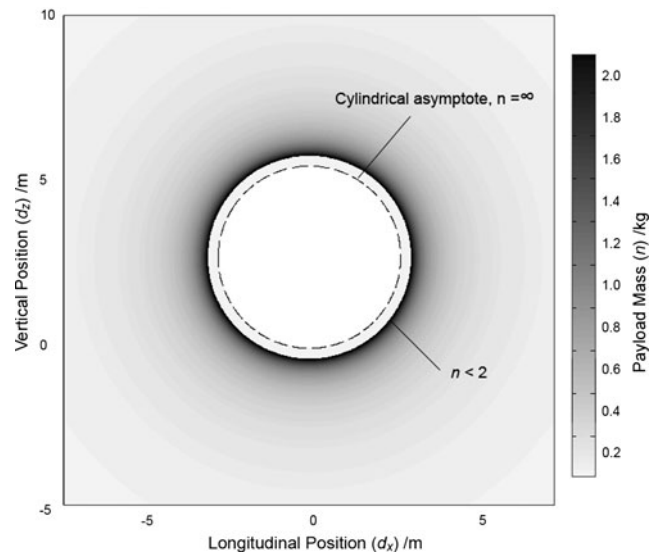


**Fig. 5** Stability region for offset loads position-mass, height map

the inequality; we denote this variable  $Q$ . Thus, any loading configuration will be stable provided that  $Q > P$ . This stability criterion  $Q$  is a physical characteristic of the vehicle relating rotor cyclic torque to rotational acceleration, and has units of  $s^{-2}$ . It appears in (2) as the open-loop pitch transfer function gain:

$$\frac{\theta(s)}{\beta(s)} = Q \frac{1}{s^2} \tag{18}$$

Stability criterion (17) can be directly transformed into a relation between the three load attributes:

$$\frac{(m+n)g(h + \frac{n}{m+n}d_z)}{I + n(d_x^2 + d_z^2)} > P \tag{19}$$

The rotational inertia of the load,  $I_n$ , is considered to be very small and is treated as zero. This relation can be solved to compute the range of permissible offsets, given a known payload mass, or conversely for maximum load given a payload position envelope.

The surface of the stability bound  $Q = P$  is a hyperbolic cylindrical funnel (Figs. 4 and 5); loading configurations under this surface are stable. The funnel is centered around  $d_z = g/2P$  with a circular asymptote (Fig. 5) of radius:

$$\sqrt{\frac{4Ph + g^2}{4P^2}} \tag{20}$$

Within this circle, no amount of added mass will destabilize the vehicle. Note that the numerical values in Figs. 4, 5, and 6 are from the T-Rex 600 helicopter and the standard controller described in Sect. 3 below, but the general shape holds for a wide range of helicopters and controllers.

In practice, the distribution of payload on a helicopter with a ventral gripper has much less variation in  $d_z$  than  $d_x$  due to the fixed height of the gripper below the helicopter.

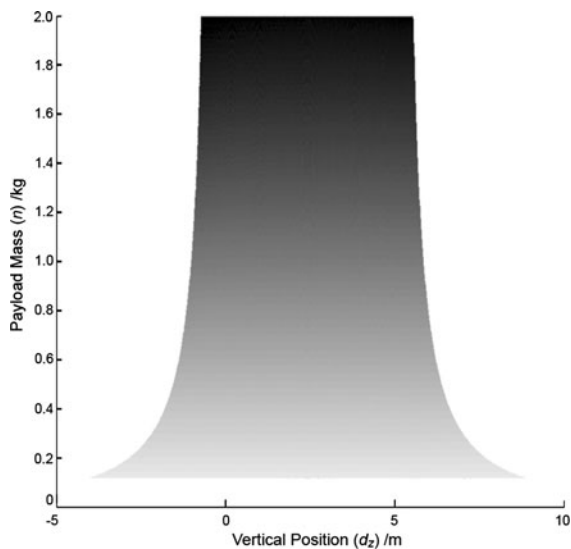


**Fig. 6** Stability region for offset loads vertical position-mass, elevation

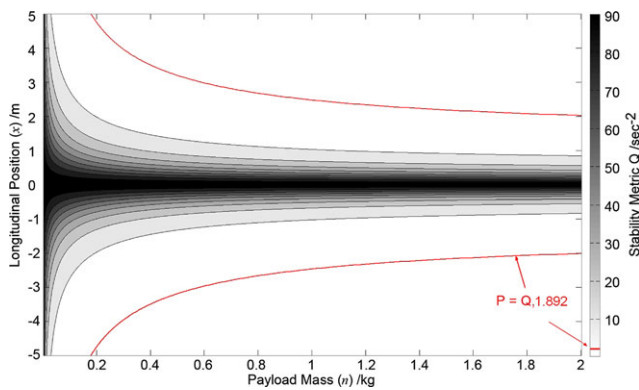


**Fig. 7** Stability metric position-mass isoelines,  $d_z = 0.2$  m

The boundary of the cross-section through the stable configuration region can be determined by holding  $d_z$  fixed:

$$d_x^2 < \left( \frac{mgh - PI}{P} \right) \frac{1}{n} + \frac{gh + gd_z - Pd_z^2}{P} \tag{21}$$

Correspondingly, the hyperbolic asymptote (Fig. 7) is given by:

$$d_x = \sqrt{\frac{h + d_z - Pd_z^2}{P}} \tag{22}$$

Similarly to (20), any mass (up to the capacity of the vehicle) may be added without destabilizing the aircraft.

Beyond predicting stability, the  $Q$  metric provides an indication of the robustness of the system. The value of  $Q$  decreases monotonically as  $d_x$  and  $n$  approach the stability bound at  $Q = P$  (Fig. 7).

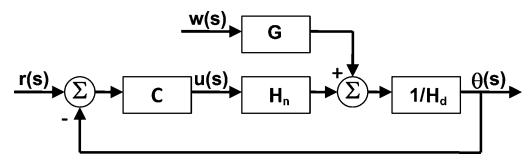


**Fig. 8** System disturbance block diagram

### 2.3 Load offset bias torque rejection

Given loading conditions known not to compromise the dynamic stability of the vehicle in flight, it can be shown that the steady-state bias torque accompanying payloads offset from the CoG will be rejected by the controller. Solving the linearized equations in the  $s$ -domain, the aircraft pitch angle can be written as a sum of the open loop system transfer function and a filtered load disturbance (Fig. 8):

$$\theta(s) = \frac{m^2ghsu(s) + Gw(s)}{IGs^2 + mghq_2Gs - m^2g^2hq_1(q_2s - 1)} \tag{23}$$

where  $G = (ms + q_1mg)$ . This can be rewritten as:

$$\theta(s) = \frac{H_n}{H_d}u(s) + \frac{G}{H_d}w(s) \tag{24}$$

As the system is linear, the two transfer functions can be considered separately. In closed-loop control with linear compensator  $C$ , the transfer function between the disturbance and the output is:

$$\frac{\theta(s)}{w(s)} = \frac{G}{H_d + CH_n} \tag{25}$$

The denominator is identical to that of the stabilized closed loop transfer function between reference,  $r$ , and the output:

$$\frac{\theta(s)}{r(s)} = \frac{CH_n}{H_d + CH_n} \tag{26}$$

Thus, the stability of the disturbance response is not dependent upon  $G$ . Given a compensator that successfully regulates the attitude dynamics around hover, small torque bias disturbances that do not take the system into the nonlinear regime or saturate the cyclic control margin will be rejected.

As  $G$  contains the non-zero constant  $q_1mg$ , the numerator of the disturbance transfer function (after a pole-zero cancellation at the origin) will not act as a pure zero:

$$\begin{aligned} \frac{\theta(s)}{w(s)} &= m(s + q_1g) \\ &\times ((m^2g^2hq_1 + Ims^2(s + q_1q) + m^2ghq_2s^2) \\ &+ m^2gh(kk_d s^2 + ks + kk_i)) \end{aligned} \tag{27}$$

Consequently, the response to a bias disturbance, while stable, will not decay to zero. This has substantial implications for robot aircraft adding and removing payload.

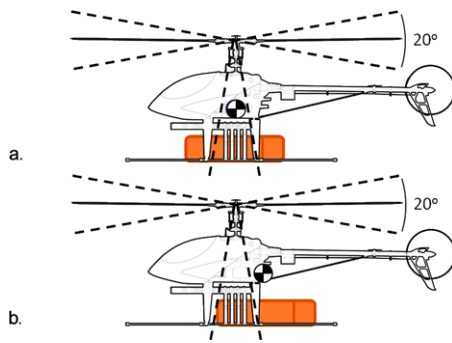


**Fig. 9** Cyclic control limits of a helicopter: center of mass inside (a) and outside (b) cyclic range

#### 2.4 Flight trim with offset payload

Conventional helicopter balancing places the payload's center of mass coaxial with the rotor shaft so that the thrust force is aligned with the load. Due to the positioning error inherent with aerial grasping, the payload may be significantly off-center when captured. An offset load weight force and the rotor thrust produce a torque couple that acts to destabilize the aircraft (Raz et al. 1988).

In flight, small imbalances can be trimmed out by adjusting the cyclic blade pitch inputs so that the thrust vector is tilted to pass through the true center of mass. One degree of cyclic blade pitch results in one degree of thrust angle deflection (Leishman 2006, p. 182). A typical small helicopter has a useful blade pitch range of 20 degrees (Prouty 2002), which requires that the center of mass of the helicopter-gripper-object system fall within a cone of approximately 10 degrees from the rotor axis (Fig. 9a). However, utilizing the full range of cyclic control to actively trim out load offsets comes at the expense of limited maneuvering control.

An unbalanced helicopter has less 'maneuvering margin,' the available cyclic range to affect maneuvers (Leishman 2006). If the payload is sufficiently imbalanced, its center of mass may be so far from the rotor axis that cyclic rotor trim cannot compensate; if the combined center of mass of the system lies outside of the cyclic cone, no degree of applied control will stabilize the vehicle in flight (Fig. 9b).

When an unbalanced load is added to the helicopter, the trim position during hover is affected. From (2), by inspection the equilibrium condition occurs when:

$$m'g\beta + m'gu = \frac{w}{h'} \quad (28)$$

Substituting into (1), the lateral acceleration becomes:

$$m'\ddot{x} = -\frac{w}{h'} - m'g\theta \quad (29)$$

As the onboard controller seeks to return  $\theta$  to zero in equilibrium, this will result in constant longitudinal acceleration. Human pilots trim for this imbalance by allowing non-zero values of  $\theta$  in hover.

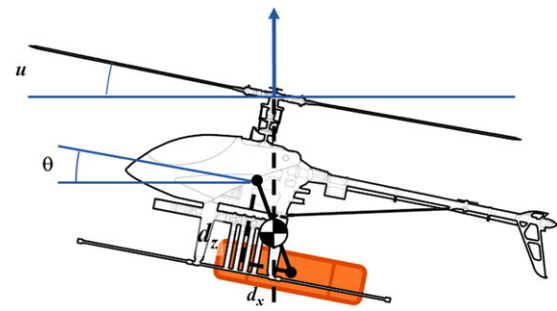


**Fig. 10** Cyclic trim balance angle

For simple weight load torque  $w = ngd_x$ , this gives the trim condition:

$$mg\theta = ng \frac{d_x}{h'} \quad (30)$$

which yields:

$$\theta = \frac{d_x}{h \frac{m}{n} + h + d_z} \quad (31)$$

This is the angle subtended by the rotor axis and the combined CoG—the trim condition where the net mass is suspended directly below the rotor hub in hover (Fig. 10).

If the mass and attachment position of the payload is known *a priori* or actively sensed, the flight controller can be instructed to maintain this pitch angle and so avoid unbounded position drift.

For level hover,  $u = -\theta$ , and this trim angle must always be within the helicopter's cyclic control range. If the cyclic control saturates, the helicopter will be uncontrollable. Typical cyclic range for a small scale helicopter is  $\pm 10^\circ$  (Prouty 2002). The cyclic range places a static load bound on the allowable mass distribution, with an asymptote at:

$$d_x = \theta(h + d_z) \quad (32)$$

where  $d_z < h$ .

#### 2.5 Cyclic range dynamic saturation

Sections 2.3 and 2.4 showed that the step disturbance introduced by instantaneously adding an imbalance load will be rejected provided the cyclic range of the helicopter is not saturated by the control response. When the system combined center of mass lies exactly on the edge of the cyclic cone, the steady-state control input  $u$  will equal the maximum cyclic deflection angle.

However, the oscillatory response of the controller to adding a mass near this limit can lead to transient  $u$  saturation, during which the guarantees of linear systems theory do not hold. The response of  $u$  to an applied load is:

$$\frac{u(s)}{w(s)} = -\frac{C_n G}{(C_d H_d + C_n H_n)} \quad (33)$$

The load response is a fourth order system, comprising a pure integrator derived from  $C$  and  $H_n$ , a near-origin zero, a fast pole and closely matched oscillatory pole-zero pair. The fast pole dominates the early response of the system, with the oscillatory dynamics contributing relatively little—less by an order of magnitude.

The initial response is approximately:

$$\frac{u(s)}{w(s)} \approx \frac{kk_d}{I(s+p)} \tag{34}$$

where  $p$  is the single real pole of  $(C_d H_d + C_n H_n)$ , found by transforming the system in the form  $s(s^3 + b_1 s^2 + b_2 s + b_3)$  into  $s(s+p)(s^2 + 2\zeta\omega_n s + \omega_n^2)$ . Solving gives:

$$p = \frac{1}{3}b_1 + \frac{1}{6}X - 6\left(\frac{1}{3}b_2 - \frac{1}{9}b_1^2\right)\frac{1}{X} \tag{35}$$

where

$$X = \left[12(12b_2^3 - 3b_2^2b_1^2 - 54b_2b_1b_3 + 81b_3^2 + 12b_3b_1^3)^{\frac{1}{2}} - 36b_2b_1 + 108b_3 + 8b_1^3\right]^{\frac{1}{3}} \tag{36}$$

for

$$b_1 = q_1g + (q_2 + kk_d)Q \tag{37}$$

$$b_2 = kQ \tag{38}$$

$$b_3 = (kk_i + q_1g)Q \tag{39}$$

Provided that  $(kk_d/Ip)w$  is within the cyclic range, the system will not experience dangerous saturation. Within the range of permissible dynamic bound payload configurations, this is satisfied everywhere the cyclic trim bound is satisfied.

The uncanceled integrator is a consequence of the translational instability of  $x$  due the constant torque imbalance. Adjustment of flight trim as described in Sect. 2.4 counters this effect. If left unchecked, the vehicle would accelerate, leading to increasing flapping countered by more cyclic, until higher-order effects such as fuselage drag restore equilibrium, or the cyclic saturates.

### 3 Numerical results and sensitivity analysis

In order to provide greater insight into analytic solutions described above, in this section we examine the stability bounds for two real helicopter UAVs and controllers. The mechanical and control parameters for the Align T-Rex 600 (used as the base platform for the Yale Aerial Manipulator (Pounds et al. 2011)) and the Yamaha R-50 (which is more than 10 times larger in mass) are given in Tables 1 and 2.

In the subsections below, we consider at the numerical dynamic and cyclic trim stability bounds for the T-Rex 600 (Sect. 3.1), and examine the sensitivity of those bounds to changing controller parameters (Sect. 3.2). Finally, we compare the results for the T-Rex 600 to the much larger R-50 (Sect. 3.3).

**Table 1** T-Rex 600 parameters

Aerodynamics and mass parameters					
$g$	9.81	$\text{m s}^{-2}$	$m$	4	kg
$h$	0.2	m	$I$	0.1909	kg m
$q_1$	0.0039		$d_z$	0.275	m
$q_2$	0.0266				
PID control parameters					
$k$	0.24		$k_d$	1.7	
$k_i$	0.7				

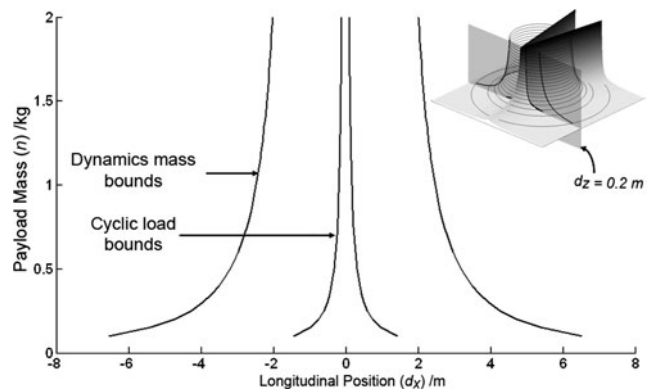


**Fig. 11** Longitudinal position-mass stability bounds for  $d_z = 0.2$  m

#### 3.1 T-Rex 600 stability bounds

As described earlier, the dynamic bounds of the T-Rex 600 (with the physical parameters and controller gains given in Table 1) are shown in Figs. 4, 5, and 6, with the stability metric  $Q$ , plotted as a function of payload mass and longitudinal position, shown in Fig. 7.

However, the cyclic trim bounds must also be taken into account. Combined with (22), the cyclic trim bound of (31) describes the range of allowable payload mass and position parameters (Fig. 11). Of the two bounds, the cyclic trim applies a much stricter limit on payload position than the dynamic stability bounds (Fig. 12). With limited cyclic control authority, the range of allowable payload positions, and the effect on dynamics stability, is expected to be small.

#### 3.2 Sensitivity to control gains

The  $P$  boundary is dependent on both physical helicopter parameters and gains of its flight controller. Mechanical constants of the aircraft, such as rotor parameters  $q_1$  and  $q_2$ , and the height of the rotor hub  $h$ , do not vary significantly in operation. Control gains, however, are subject to variation as the controller is adjusted between missions (and some controllers may also permit adjustment during flight).

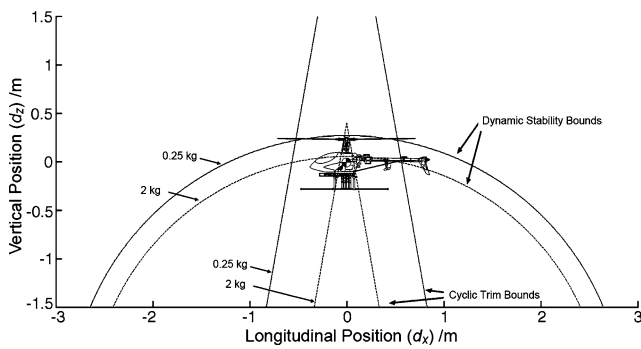


**Fig. 12** Position stability bound isoclines for 0.25 and 2 kg loads

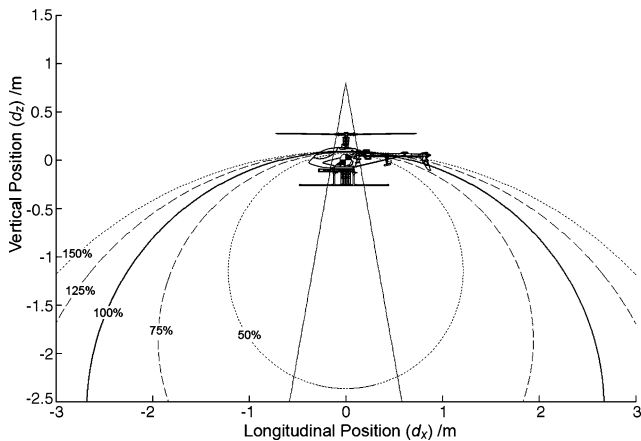


**Fig. 13** 1 kg payload bounds with changing proportional flight control gain

A range of helicopter flight controller gains can be chosen depending upon the desired performance of the vehicle for a given task or loading condition. Figures 13, 14 and 15 show how variations in the proportional, integral, and derivative controller gains affect the dynamic payload stability bounds, respectively. Sensitivity of a helicopter's stable loading configuration to parameter adjustment is generally low. However, it can be seen that, in terms of the controller gains tuned to give good performance of the T-Rex 600, variations in the proportional and derivative gains have a much greater effect on the stability bounds than the integral term. Only extremely small gain values will produce dynamic stability bounds more stringent than those imposed by the cyclic pitch limit, which does not change with varying control parameters, and these may be unstable in free flight.

### 3.3 Mass scaling

Scaling up to a larger aircraft increases the amount of payload that can be carried. For payloads of a fixed proportion of aircraft mass, the  $Q$  metric remains constant with changing weight. However, required rotor height increases quadratically with increase in payload offset; the bound due

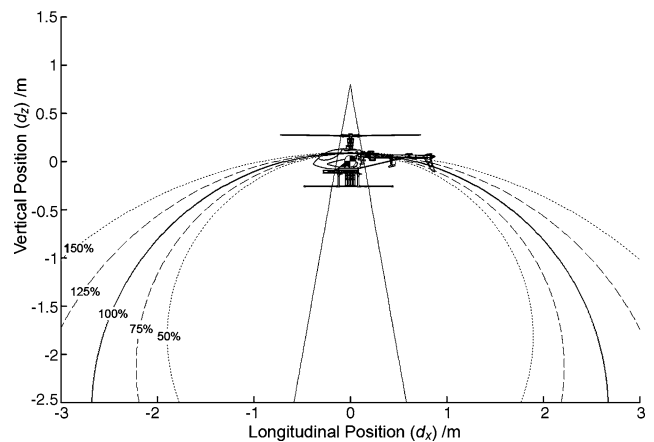


**Fig. 14** 1 kg payload bounds with changing integral flight control gain

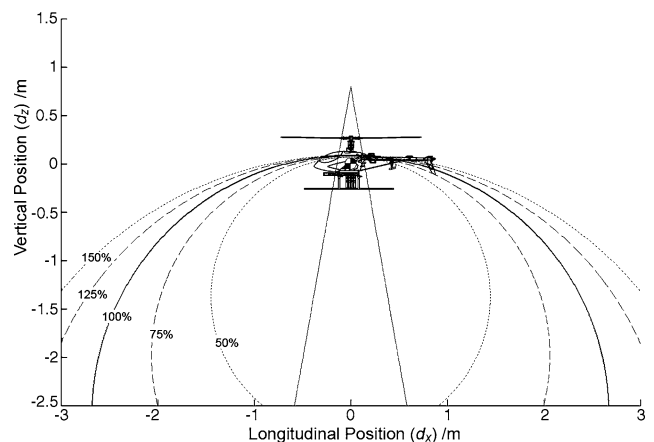


**Fig. 15** 1 kg payload bounds with changing derivative flight control gain

to cyclic limit is linear. Consequently, although a larger helicopter will have a smaller dynamic bound, it will have a larger cyclic bound.

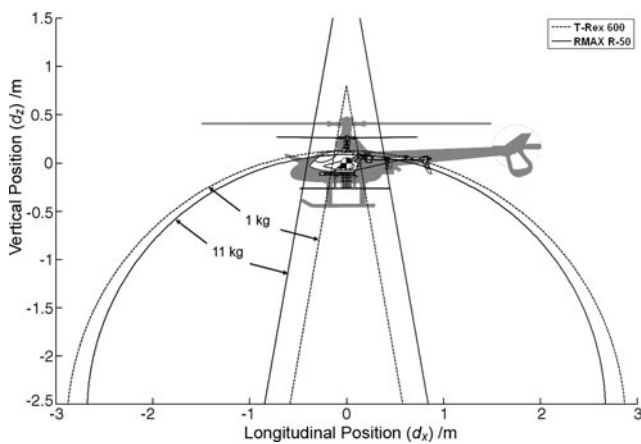
To make a comparison between differently sized aircraft, a vehicle with a similar main rotor speed (and thus Froude Number) is chosen: the Yamaha R-50 industrial UAV. The R-50 weighs 44 kg, approximately 10 times the mass of the T-Rex 600, with rotor speed of  $86 \text{ rad s}^{-1}$ . Parameters of the R-50 taken from Mettler (Mettler 2003) and Enns and Keviczky (Enns and Keviczky 2006) are given in Table 2. No information on the cyclic range of the R-50 was available, but it is expected to be approximately  $10^\circ$ , like the majority of helicopters. The control parameters of the two systems are similar, with the exception of slightly greater system gain of the R-50.<sup>3</sup>

In the case where the T-Rex 600 and R-50 are loaded with payload 25 per cent of their unladen mass (1 kg and 11 kg,

<sup>3</sup>The R-50 control structure does not use a pure integral term—its integral action is derived from position. The value of  $k_i$  used is inferred.

**Table 2** R-50 parameters

Aerodynamics and mass parameters					
$g$	9.81	$\text{m s}^{-2}$	$m$	44	kg
$h$	0.573	m	$I$	9.99	kg m
$q_1$	0.002		$d_z$	NA	m
$q_2$	0.0151				
PID control parameters					
$k$	0.29		$k_d$	1.5	
$k_i$	0.75				

**Fig. 16** R-50 and T-Rex 600 loading bounds for payloads 25 per cent of vehicle mass

respectively), it can be seen that the R-50's useful horizontal payload offset is approximately 50 per cent wider than that of the T-Rex 600 (see Fig. 16). Simple linear scaling would predict a 67 per cent increase; the slightly lower value is due to differences in rotor and gain values.

#### 4 Stability to payload offset experiments

Validation of the analysis warrants experimental verification of changing helicopter stability under PID control after payload capture. However, probing stability bounds is both challenging and potentially unrecoverable. In the case of a real helicopter in free flight, it is generally not possible to recover the system after going unstable, naturally preventing operation in unsafe regions. Furthermore, as even small wind drafts will disturb small vehicles, it is nearly impossible to establish constraints desirable for experimental analysis, and even the best sensory suites for unstructured outdoor environments (where systems such as Vicon are unavailable) have a relatively slow response and low sensitivity.

Consequently, we have taken the approach of showing basic validation of the analytical results by performing nu-

**Fig. 17** Yale Aerial Manipulator with payload rail and fixed gear

merous experimental trials in real, unstructured environments. These demonstrate aircraft stability and bias rejection for predicted stable configurations. Identified system responses of the vehicle for a range of loadings is shown to follow the trend expected as the system moves towards instability, within the bounds of what is reasonably tractable in unstructured outdoor environments.

Two experiments were performed: the first to demonstrate robustness of the flight controller to changing step loads (with fixed position) and the second to assess stability of the controller with changing payload positions (and fixed mass).

#### 4.1 Experimental platform

Our experimental platform is the 4 kg, 1.5 m rotor, T-Rex 600 ESP radio control helicopter (Align, Taiwan) (see Fig. 17). The helicopter is fitted with a Helicommand Profi flight stability system that employs a PID attitude controller, with known parameters. It also controls height above ground and position drift using optical feedback, but this function is turned off during experiments to avoid interference with dynamic response measurements. Flight attitude is measured by a 3DM-GX3-25 inertial measurement unit (Microstrain, Vermont USA) and transmitted via Bluetooth to an off-board laptop.

A 0.48 m long aluminum rail is mounted ventrally between the helicopter's skids, 0.2 m below the unladen aircraft CoG, aligned with the aircraft  $x$  axis (see Fig. 17). The rail has mounting holes every 25.4 mm to which a fixed mass or remote-triggered electromagnet may be secured, allowing loads to be shifted between tests, or dropped mid-test.

#### 4.2 Induced load bias test

In the first experiment, a 0.125 kg test mass was dropped from a range of mounting positions under the helicopter to

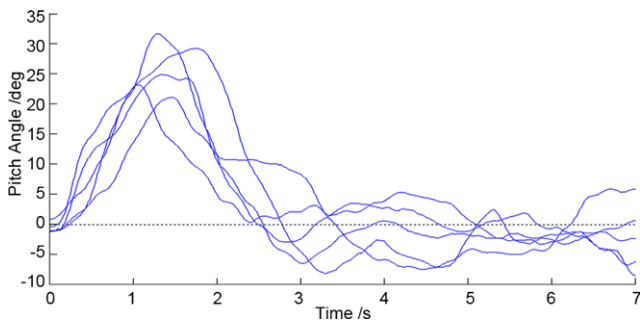


**Fig. 18** Normalized unit load bias step responses

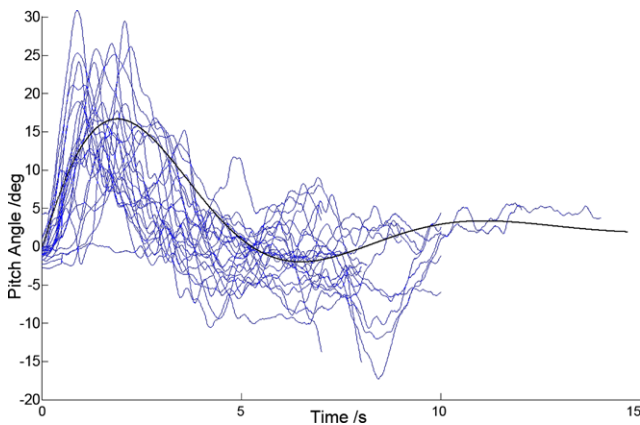


**Fig. 19** Normalized shifted mass drop step responses

produce a step load disturbance. From (28), rotor cyclic control is analogous to applied torque—by trimming the aircraft in flight with the test mass in place and then releasing it, the pitch dynamics will emulate the effect of instantaneously applying an unbalanced payload.

Prior to the drop, the helicopter is autonomously held stationary out of ground effect, at a pitch angle that cancels the moment of the test mass. As the drop is triggered, the horizontal position control of the flight stabilizer is simultaneously disabled.

The resulting pitch motion of the aircraft shows that the system successfully rejects step biases (see Fig. 18). Five trials were performed, with the test mass 50.8 mm forward of rotor axis and moved 50.8 mm further from the rotor axis each time. As expected from (29), however, the lateral motion of the aircraft was unbounded and experiment settling time was limited by available flight space.

#### 4.3 Added mass flight stability test

In the second experiment, an offset payload is added to the helicopter to assess stability of the controller with changing payload configurations. The payload is fixed at a range of locations on the mounting rail, and the helicopter is trimmed for the added weight, along with a smaller test mass at a

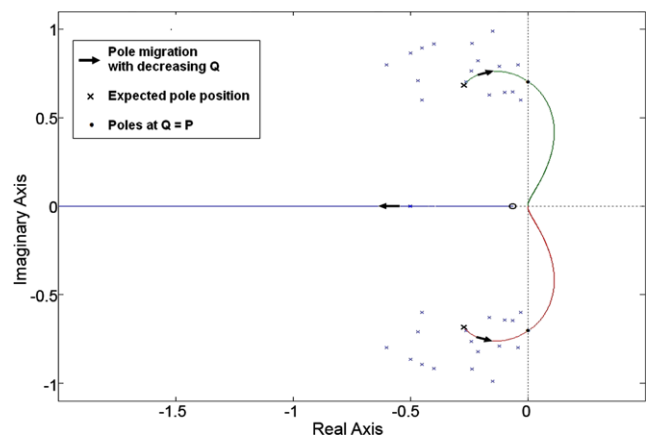


**Fig. 20** Shifted mass step response pole positions

fixed location. The experiment setup is as previously: the aircraft is kept stationary under autonomous control until the test mass is released to induce a step response. In total, 24 trials were performed, with the fixed mass moved 25.4 mm further from the rotor axis, every third trial.

From (25), the expected disturbance step response is a one zero, three pole system with a decaying oscillation period of 7.6 s. Due to limited airspace for testing, not all tests could be allowed to continue to complete settling.

In outdoor flight, the pitch motion of the aircraft is noisy, making estimation of the system poles difficult. Some cross-coupling between pitch and roll was observed; a least-squared regression on roll measurements identified a linear coupling factor and phase lag that was used to remove its influence in the pitch measurement.

The aggregate dynamics tracked the predicted step response of the system (see Fig. 19), with a slightly shorter oscillation period than predicted ( $\sim 5$  s). Given the noise in the measurements, the oscillatory poles of the step responses were widely spaced; they are shown super imposed on the root locus with respect to changing  $Q$  in Fig. 20. As  $Q$  decreases, the system is expected to become more oscillatory, crossing the axis when  $Q = P$ . However, the limitation imposed by (31), prevented the mass from being displaced far enough to discern any trend towards incipient instability.

## 5 Quadrotor stability with changing payload

The stability analyses presented in Sect. 2 can be straightforwardly extended to quadrotors, which are popular experimental platforms for UAV researchers. Unlike conventional helicopters, quadrotors do not use a cyclic blade pitch control to effect manoeuvres, but rather use speed changes between pairs of rotors to induce control torques. Also, the small, high-speed rotors of quadrotors induce proportionally less flapping than full-scale helicopters. Consequently, the

**Table 3** X-4 Flyer parameters

Aerodynamics and mass parameters					
$g$	9.81	$\text{m s}^{-2}$	$m$	4.34	kg
$h$	-0.007	m	$I$	0.084	kg m
$d$	0.32	m	$u_{\max}$	2.95	N m
PID control parameters					
$k$	4.6		$k_d$	0.3	
$k_i$	0.2				

dynamics of a quadrotor with changing load conditions are distinctive.

While numerous techniques have been developed for controlling quadrotor flight angle, standard PID controllers are popular and effective (Pounds et al. 2010; Bouabdallah et al. 2004). By choosing a quadrotor of similar size, payload capacity, and controller architecture to the T-Rex 600 analyzed above, the differences in the stability bounds for the two platform architectures can be compared.<sup>4</sup>

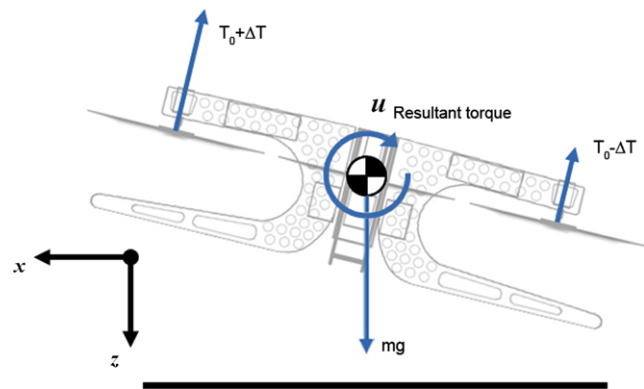
For our purposes, we will consider the ANU X-4 Flyer, an unusually large 4 kg quadrotor with similar payload capacity to the T-Rex 600; although the X-4 is fitted with explicit mechanical flapping hinges, its flapping coefficients are much smaller ( $q_1 = 0.0015$  and  $q_2 = 0.013$ ) and can be effectively ignored. Its parameters are given in Table 3.

### 5.1 Quadrotor dynamic model

Dynamic modeling and control of quadrotors is a well-studied problem (Borenstein 1992; Pounds et al. 2010; Bouabdallah et al. 2004; Hamel et al. 2002). While the core mechanics of quadrotors are very similar to helicopters, there are two key differences. Firstly, the tip-path plane of a rotor is largely constant for small quadrotors in low-speed flight. The direction of rotor thrust always remains perpendicular to the rotor shaft—no off-axis forces are applied to the vehicle. This separates the cross-coupling between cyclic control input and translation, and between translational velocity and pitch, greatly simplifying the dynamics (see Fig. 21).

Secondly, the horizontal displacement of pairs of rotors from the center of gravity of the aircraft causes the rotors to move vertically through the rotor air stream as the vehicle pitches and rolls (Pounds et al. 2010). This vertical motion relative to the vertical wind changes the local observed angle of attack of the blade airfoils. A rotor moving upwards

<sup>4</sup>Compared with helicopters of the same mass, quadrotors have significantly smaller rotors with faster blade tip speeds, making the Froude Numbers very different. Furthermore, unlike small platforms, larger quadrotors more strongly exhibit flapping, complicating the comparison.

**Fig. 21** Quadrotor free body diagram

experiences a decrease in thrust, while a rotor moving downwards experiences an increase in thrust—the resulting thrust differential opposes the direction of rotation, damping the motion. This damping effect can be an order of magnitude greater than the similar effect from rotor flapping due to pitch and roll.

The rigid-body dynamics of a simplified linearized planar quadrotor in hover are:

$$m\ddot{x} = -mg\theta \quad (40)$$

$$I\ddot{\theta} = -q_3\dot{\theta} + u + w \quad (41)$$

where  $q_3$  is a rotor inflow damping constant, and in this case  $u$  is the pitch torque control input. Flapping effects are treated as negligible and ignored.

The longitudinal transfer function between torque input and pitch angle is straightforward to compute, as horizontal translation is decoupled:

$$H = \frac{1}{Is^2 + q_3s} \quad (42)$$

### 5.2 Flight stability with payload mass

Like conventional helicopters, quadrotors are regularly stabilized in attitude with PID flight controllers. As before, the stability of the resulting system can be demonstrated with linear systems analysis. Unlike cyclic-controlled helicopter, quadrotors do not exhibit flapping term cancellation that reduces their dynamics to third order. If flapping mechanics are excluded, pitch dynamics are naturally second order. Consequently, stability analysis is much simpler, and has no dependency on mass or the height of the rotor above the CoG.

The characteristic polynomial for a quadrotor with PID stabilization is:

$$s^3 + \frac{1}{I}(q_3 + kk_d)s^2 + \frac{k}{I}s + \frac{kk_i}{I} \quad (43)$$

Stable third order polynomials of the form  $s^3 + a_1s^2 + a_2s + a_3$  require that all coefficients be positive and that  $a_1a_2 -$

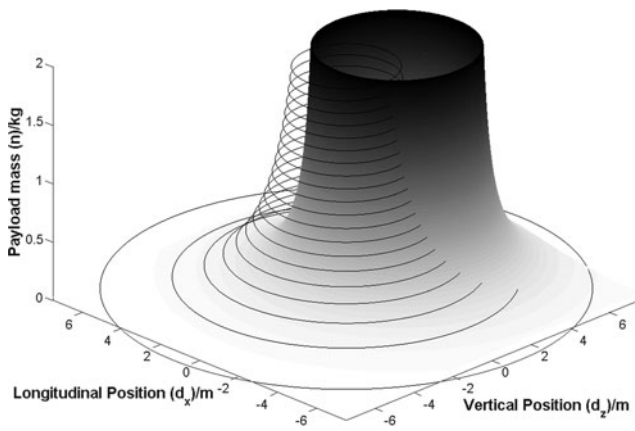


**Fig. 22** X-4 Flyer dynamic stability isoclines and T-Rex 600 dynamic stability surface (shaded)

$a_3 > 0$ . This produces a stability criterion in the form similar to that of (17):

$$\frac{1}{I'} > \frac{k_i}{q_3 + kk_d} \tag{44}$$

Unlike (17) quadrotors are not sensitive to change in cyclic control torque scaling due to vertical shift of the center of mass. Consequently, the surface of the stability bound is centered around the unladen vehicle’s center of mass, rather than below it (see Fig. 22). This makes quadrotors more suitable than helicopters for conditions where the aircraft must be loaded high in the airframe. A related case for raising the center of mass of quadrotors to improve control performance was described previously (Pounds et al. 2010).

For the same reasons, quadrotors have a pure hyperbolic asymptote at the CoG; there is no circular region of insensitivity to load mass, making them more sensitive to the displacement of heavy loads. However, the inflection of the stability surface is less than that for helicopters and so quadrotors like the X-4 Flyer are less sensitive in the range of loads that are typically carried. At the X-4 Flyer’s 1 kg payload capacity, the permissible offset range is similarly sized with the T-Rex 600 (see Fig. 23).

5.3 Load offset bias torque rejection

The disturbance transfer function is similarly derived as per conventional helicopters. The linearized system is of the form:

$$\theta(s) = \frac{1}{H_d}u(s) + \frac{1}{H_d}w(s) \tag{45}$$

where control input and load disturbance have the same unit numerator. In closed loop, the sensitivity function is:

$$\frac{\theta(s)}{w(s)} = \frac{1}{1 + CH_d} \tag{46}$$

which once again has the same denominator of the closed-loop pitch dynamics, and is thus stable. Unlike the case of

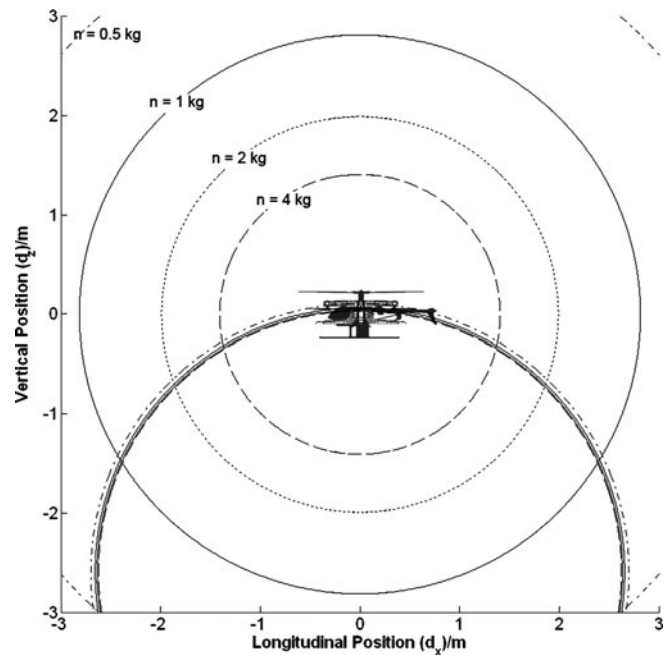


**Fig. 23** X-4 Flyer and T-Rex 600 dynamic stability isoclines

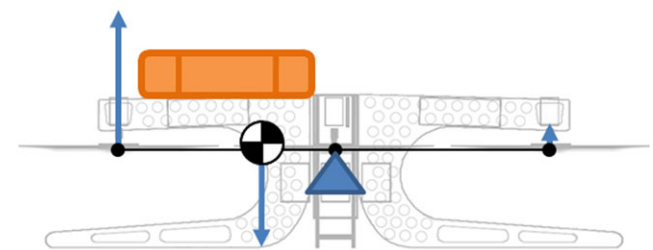


**Fig. 24** Quadrotor force balance in trim

helicopter, the lack of quadrotor flapping<sup>5</sup> results in the disturbance step response decaying to zero:

$$\frac{\theta(s)}{w(s)} = \frac{s}{Is^3 + (q_3 + kk_d)s^2 + ks + kk_i} \tag{47}$$

5.4 Flight trim with payload offset

Unlike conventional helicopters, planar quadrotors develop lifting thrust at two points on the aircraft and do so in a constant vertical direction. Load imbalances are adjusted for by changing the relative proportion of the thrusts (whilst keeping the overall magnitude of thrust constant). Of particular interest for robotics applications of hovering aircraft, quadrotors can maintain horizontal flight attitude even with unbalanced loads, without necessarily producing lateral thrust (see Fig. 24).

The permissible static imbalance torque  $w = nd_x$  is limited by the maximum increase or decrease in rotor speed,  $\delta\omega$

<sup>5</sup>In practice all rotorcraft exhibit flapping, however small.

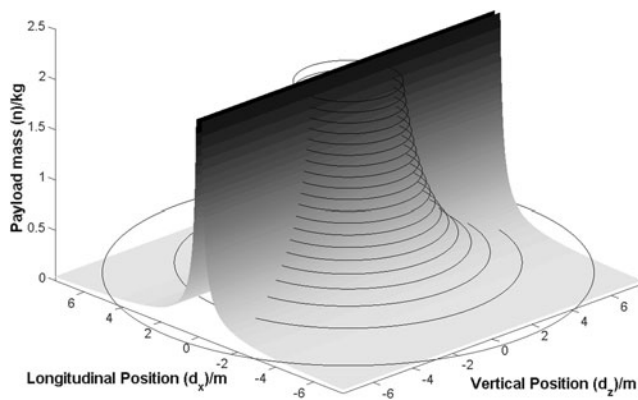


**Fig. 25** Quadrotor trim stability boundary

and the distance of the rotor hubs from the unladen center of gravity,  $d$ , which produce a maximum achievable torque  $u_{\max} \propto \delta\omega^2$ :

$$0 = u_{\max} - n g d_x \quad (48)$$

This hyperbolic relation has asymptotes at  $d_x = 0$  and  $n = 0$ , but does not depend on vertical offset of the added mass (see Fig. 25).

Compared with a conventional helicopter the range of lateral offsets that may be accommodated is quite small, significantly less than the cyclic stability cone below the rotor (see Fig. 26). Although a quadrotor may achieve substantial thrust, the unidirectional thrust of opposing motors acts to limit the maximum reaction torque that can be applied—only a relatively small difference in thrust may be leveraged. However, quadrotors designed for carrying loads can increase their permissible payload offsets by increasing  $d$ , which is a much simpler modification than changing rotor mast height on a traditional helicopter.

## 6 Conclusion

In this paper we have presented planar helicopter and quadrotor models and analyzed attitude stability subject to bias and step disturbance encountered during instantaneous payload change and offset loadings. We have shown that under PID control, a helicopter will successfully reject added load offsets within a fairly large range, and that cyclic trim limitations dominate the range of allowable load positions. Successful helicopter loading configurations are insensitive to parameter variation in their flight control, or substantial changes in mass, as the bounds of cyclic range dominate under even a large range of controller gain configurations.

Experimental results with a test vehicle confirmed pitch stability of the helicopter under trim imbalance, and also demonstrated predicated unbound lateral translation. Note

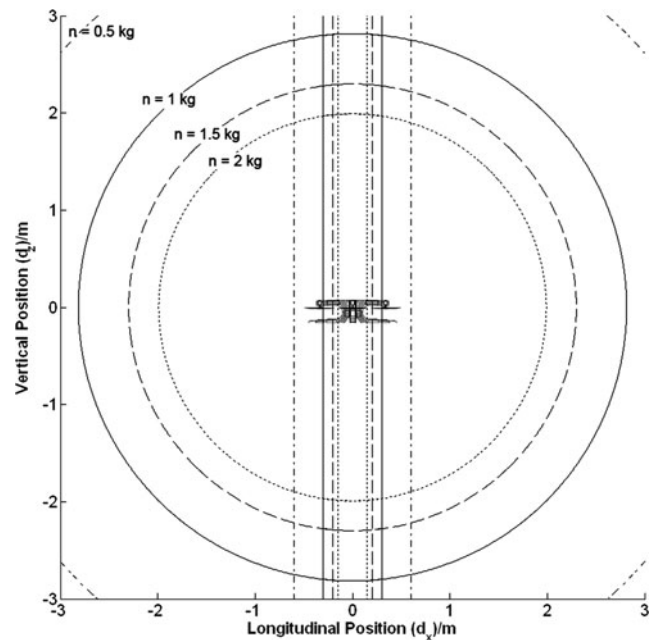


**Fig. 26** Combined quadrotor stability isoclines

for a fully autonomous helicopter system, so means of measuring and correcting for this lateral translation must be implemented in the controller, such as through the use of optical flow measurements of motion relative to ground, a capability that exists in high-end off-the-shelf controllers such as the Helicommand Profi.

Quadrotors were found to exhibit stable pitch dynamics and bounded lateral translation under bias loading. While quadrotors have a much smaller range of permissible load placement offsets, they offer stable loading configurations directly on top of the airframe, compared to helicopters, where loads must be added close to, or below, the unladen center of gravity. This makes quadrotors an attractive option for robotic payload carrying tasks where the load is added from above. Additionally, due to the ability to adapt to payload offsets through rotor speed differential, quadrotors do not exhibit the unbounded lateral translation seen in uncompensated standard helicopters.

**Acknowledgements** The authors would like to thank Joe Acosta of Build Right Fly Right Hobbies, Wallingford CT, USA, Greg Brown and Joseph Belter for their support of this work. This work was supported in part by the Office of Naval Research grant N000141010737.

## References

- Amidi, O., Kanade, T., & Miller, J. (1998). Vision-based autonomous helicopter research at Carnegie Mellon Robotics Institute 1991–1997. In *Proc. American Helicopter Society international conference*.
- Bernard, M., & Kondak, K. (2009). Generic slung load transportation system using small size helicopters. In *Proc. IEEE international conference on robotics and automation*.

- Bisgaard, M., Bendtsen, J., & la Cour-Harbo, A. (2009). Modelling of generic slung load system. *Journal of Guidance, Control and Dynamics*, 32(2), 573–585.
- Borenstein, J. (1992). The Hoverbot—an electrically powered flying robot. Unpublished paper, University of Michigan. <http://www-personal.umich.edu/~johannb/hoverbot.htm> (2009).
- Bouabdallah, S., Noth, A., & Siegwart, R. (2004). PID vs LQ control techniques applied to an indoor micro quadrotor. In *Proc. IEEE/RSJ international conference on intelligent robots and systems*.
- Enns, D., & Keviczky, T. (2006). Dynamic inversion based flight control for autonomous RMAX helicopter. In *Proc. American controls conference*.
- Hamel, T., Mahony, R., Lozano, R., & Ostrowski, J. (2002). Dynamic modelling and configuration stabilization for an X4-Flyer. In *Proc. 15th triennial world congress of the International Federation of Automatic Control*.
- Kuntz, N., & Oh, P. (2008). Development of autonomous cargo transport for an unmanned aerial vehicle using visual servoing. In *Proc. digital systems and control conference*.
- Leishman, J. G. (2006). *Principles of helicopter aerodynamics*, 2nd edn. New York: Cambridge University Press.
- Mammarella, M., Campa, G., Napolitano, M., Fravolini, M., & Perhinschi, R. (2008). Machine vision/GPS integration using EKF for the UAV aerial refueling problem. *IEEE Transactions on Systems, Man and Cybernetics*, 38(6), 791–801.
- Mettler, B. (2003). *Identification, modeling and characteristics of miniature rotorcraft*. Nowell: Kluwer Academics Publisher.
- Michael, N., Fink, J., & Kumar, V. (2009). Cooperative manipulation and transportation with aerial robots. In *Proc. robotic science and systems*.
- Pounds, P. E. I., & Dollar, A. M. (2010). Hovering stability of helicopters with elastic constraints. In *Proc. ASME dynamic systems and control conference*.
- Pounds, P. E. I., Corke, P. I., & Mahony, R. E. (2010). Modelling and control of a large quadrotor robot. *Control Engineering Practice*, 18(7), 691–699.
- Pounds, P. E. I., Bersak, D. R., & Dollar, A. M. (2011). Grasping from the air: hovering capture and load stability. In *Proc. international conference on robotics and automation*.
- Prouty, R. (2002). *Helicopter performance, stability, and control*. Malabar: Krieger Publishing.
- Raz, R., Rosen, A., & Ronen, T. (1988). Active aerodynamic stabilization of a helicopter/sling-load system. *Journal of Aircraft*, 26(9), 822–828.
- Scott, D., Toal, M., & Dale, J. (2007). Vision based sensing for autonomous in-flight refueling. In *Proc. of SPIE* (Vol. 6561).



**Daniel R. Bersak** is a graduate student in Mechanical Engineering at Yale University. He holds a S.M. in Mechanical Engineering from Yale, a B.S. in Electrical Engineering and S.M. and B.S in Comparative Media Studies from MIT.



**Aaron M. Dollar** is Assistant Professor of Mechanical Engineering at Yale University. His research interests include robotic grasping and manipulation, tactile sensing, prosthetics and rehabilitation robotics, active exoskeletons, and robot locomotion. Prof. Dollar is an active member of the American Society of Mechanical Engineers (ASME), the IEEE, and the American Society of Engineering Education (ASEE), and is the editor and co-founder of RoboticsCourseWare.org, an open repository for robotics pedagogical materials. Prof. Dollar holds Ph.D. and S.M. degrees from Harvard University in Engineering Sciences and a B.S. in Mechanical Engineering from the University of Massachusetts at Amherst.



**Paul E.I. Pounds** is a lecturer in Mechatronics at the University of Queensland. His research focuses on rotary wing unmanned aerial vehicle dynamics, systems and control. He is a member of the IEEE and Australian Professional Scientists, Engineers and Managers Association. He holds a Ph.D. and B.E. Systems Engineering from the Australian National University. He completed his post-doc at Yale in 2011.